Metabolic network construction reveals probiotic-specific alterations in the metabolic activity of a synthetic small intestinal community

Jack Jansma [1], Anastasia Chrysovalantou Chatziioannou [1*], Kitty Castricum [2], Saskia van Hemert [2], Sahar El Aidy [1#]

Affiliations

[1] Host-microbe Interactions, Groningen Biomolecular Sciences and Biotechnology Institute (GBB), University of Groningen, Groningen, The Netherlands.

[2] Winclove Probiotics, Amsterdam, the Netherlands

*Present address: Department of Chemistry, Laboratory of Analytical Biochemistry, University of Crete, Heraklion, Greece

[#] Corresponding author

Sahar El Aidy. Host-microbe Interactions, Groningen Biomolecular Sciences and Biotechnology Institute (GBB), University of Groningen, Nijenborgh 7, 9747 AG Groningen, The Netherlands. P: +31(0)503632201.

E: sahar.elaidy@rug.nl

Abstract

The gut microbiota plays a crucial role in maintaining overall health and probiotics have emerged as a promising microbiota-targeted therapy for improving human health. However, the molecular mechanisms of probiotics action in general and the targeting of small intestinal microbiota by probiotics are not well understood. To address this, we constructed a synthetic community of three species, which resembles the upper small intestinal microbiota. Our results indicate that probiotic supplementation can directly affect the metabolism of the community, resulting in colonization resistance in a probiotic specific manner. Supplementation with *Streptococcus thermophilus* led to increased lactate production and a decrease in pH, while *Lactobacillus casei* supplementation increased the resistance to perturbations and nutrient utilization without affecting lactate production or pH. Additionally, when combined with kynurenine, *Lactobacillus casei* enhanced the kynurenine pathway metabolism resulting in elevated kynurenic acid levels and possibly indirect colonization resistance. Overall, our study reveals how selecting probiotics with distinct functional capacities can unlock the full potential of microbiota-targeted therapies.

Keywords

Small intestine, microbiota, probiotics, dynamic metabolic networks, kynurenic acid

Importance

The development of probiotic therapies targeted at the small intestinal microbiota represents a significant advancement in the field of probiotic interventions. This region poses unique opportunities due to its low number of gut microbiota, along with the presence of heightened immune and metabolic host responses. However, progress in this area has been hindered by a lack of detailed understanding regarding the molecular mechanisms through which probiotics exert their effects in the small intestine. Our study, utilizing a synthetic community of three small intestinal bacterial strains and the addition of two different probiotic species, and kynurenine as a representative dietary or endogenously

53 produced compound, highlights the importance of selecting probiotic species with diverse genetic
54 capabilities that complement the functional capacity of the resident microbiota, or alternatively,
55 constructing a multispecies formula. This approach holds great promise for the development of
56 effective probiotic therapies and underscores the need to consider the functional capacity of probiotic
57 species when designing interventions.
58
59
60
61
62
63 **Introduction**
64 In recent decades, there has been a growing interest in investigating the gut-microbiota and its
65 significant roles in maintaining human health [1, 2]. The gut-microbiota is composed primarily of
66 *Bacteroidaceae*, *Prevotellaceae*, *Rikenellaceae*, *Lachnospiraceae* and *Ruminococcaceae*, which reside
67 mainly in the colon [3]. In contrast to the colon, the small intestinal microbiota is highly dynamic and
68 location-specific. For example, *Streptococcaceae* and *Veilonellaceae* are abundant in the duodenum
69 [4], while *Streptococcaceae*, *Carnobacteriaceae* and *Actinomycetaceae* prevail in the jejunum [5] and
70 *Lactobacillaceae*, *Erysipelottrichaceae*, and *Enterobacteriaceae* are dominant in the ileum [6]. The
71 small intestinal microbiota plays a crucial role in regulating the metabolic, endocrine, and immune
72 functions of their hosts [7–9]. Consequently, altering the equilibrium between the host and the
73 microbiota can negatively affect the health of the host [10, 11]. Thus, to re-establish this equilibrium
74 and enhance the health of the host, multiple microbiota-targeted therapies, such as probiotics, are
75 employed [12].
76 Probiotics are defined as live microorganisms that, when administered in adequate amounts, confer a
77 health benefit on the host [13]. The development of probiotic therapies aiming at targeting the small
78 intestinal microbiota poses a significant challenge due to the limited access to the human small

79 intestine. Currently, investigations into the effect of probiotics on the small intestine are carried out
80 either directly on animal models [9, 14] or indirectly through small clinical trials that lack detailed
81 molecular mechanisms [15]. This lack of understanding hampers the development of novel probiotic
82 therapies. In recent years, it has been demonstrated that the microbiota retrieved from stoma effluent
83 exhibits similar compositional and behavioral characteristics with the healthy ileal microbiota [16].
84 These findings suggest that the stoma effluent-derived microbiota may serve as a promising source for
85 probiotic research [17, 18]. However, the utilization of stoma effluent is limited for the study of the
86 upper small intestine. To address this limitation, there is a need for the construction of synthetic
87 bacterial communities to bridge this research gap [19]. Synthetic bacterial communities are bacterial
88 mixtures produced through co-culturing of selected bacteria in controlled environments [20]. These
89 communities can comprise a range from two [21] to over one hundred species [22]. Synthetic
90 communities can be subjected to perturbation through manipulation of growth parameters or the
91 introduction of new bacterial species, and can also be supplemented with specific compounds such as
92 prebiotics [23]. Analysis of the community's molecular response allows a deeper understanding of the
93 underlying molecular mechanisms [24], optimization of metabolites' production [25] and assessment
94 of emergent properties such as stability or resistance to perturbations [26, 27]. This methodology has
95 the potential to guide the development of novel microbiota-targeted therapies.
96 In humans, the kynurenine pathway is the primary route for the metabolism of free tryptophan, and it
97 plays a critical role in the generation of energy in the form of nicotinamide adenine dinucleotide
98 (NAD^+), immune system regulation [28] and the production of the neuroactive compounds quinolinic
99 and kynurenic acid (KYNA) [29]. Increased tryptophan metabolism via the kynurenine pathway in the
100 gut is associated with obesity and alterations in the microbiota [29]. G-protein coupled receptor 35
101 (GPR35), which is activated by KYNA, is abundantly expressed in the intestine, where it plays a role in
102 immune regulation and epithelial barrier function [30]. The concentration of KYNA in the gut lumen
103 increases from the proximal to the distal part of the intestine, indicating production by the gut
104 microbiota [31, 32]. Several gut bacteria can produce compounds from the kynurenine pathway [32,

105 33] and probiotics supplementation have been shown to reduce intestinal inflammation and improve
106 intestinal barrier function accompanied by reduced kynurenine but increased KYNA levels [34, 35].
107 However, the precise effects of kynurenine pathway metabolism within the microbiota remain
108 unknown.

109 In the present study, a dynamic correlation-based network approach was utilized in
110 conjunction with multivariate analysis of experimental data obtained from chip-based digital
111 polymerase chain reaction (c-dPCR), proton-nuclear magnetic resonance (^{1}H-NMR) and high-
112 performance liquid chromatography-ultraviolet (HPLC-UV). The aim was to examine the impact of
113 introducing probiotic species on the general metabolic activity and the kynurenine pathway activity of
114 a simplified community consisting of three intestinal isolates, which represent the small intestinal
115 microbiota.

116

117 **Material and methods**

118 *Bacteria and growth media*

119 Bacteria were selected based on their abundance in the upper small intestine, ability to metabolically
120 affect the kynurenine pathway or probiotic activity in the small intestine. *Escherichia coli* DSM11250
121 was obtained from the German collection of microorganisms and cell cultures; *Pseudomonas*
122 *fluorescens* MFY63 was obtained from the laboratory of microbiology signals and microenvironment
123 [36]; *Streptococcus salivarius* HSISS4 was obtained from the laboratory of host-microbe interactomics
124 [37]; *Streptococcus thermophilus* W69 and *Lactobacillus casei* W56 were obtained from Winclove
125 probiotics. All individual bacterial and community growth experiments were performed using enriched
126 beef broth (EBB) [38].

127

128 *Bacterial kynurenine pathway metabolism*

129 To investigate kynurenine pathway metabolism by the bacterial strains, 3 mL EBB was inoculated from
130 a glycerol stock stored at -80 °C and grown overnight at 37 °C. *E. coli* and *P. fluorescens* were grown

131 shaking at 220 RPM, *S. salivarius*, *S. thermophilus* and *L. casei* were grown without shaking. Overnight
132 grown pre-culture were diluted 1:100 in fresh EBB supplemented with 500 µM tryptophan and
133 kynurenine or kynurenic acid. At the start (0h) and at termination of the experiment (24h) 250 µL
134 culture was transferred to a new tube and immediately 1 mL cold (-20 °C) methanol was added. The
135 samples were stored at -20 °C until further use.
136
137 *Growth experiments, community construction and sampling in a mini-bioreactor*
138 All experiments were conducted in a MiniBio 250 mL bioreactor
139 (Applikon Biotechnology, The Netherlands) with a working volume of 250 mL. Each experiment was
140 performed in 200 mL EBB + 500 µM tryptophan and, if indicated 100 µM kynurenine. To prevent foam
141 accumulation 0.1 % (v/v) silicon antifoam emulsion (Carl Roth, Germany) was added. The temperature,
142 dissolved oxygen and pH were monitored online. The adaptive my-Control system
143 (Applikon Biotechnology, The Netherlands) was used to control process parameters. Setpoints of 50%
144 of the atmospheric oxygen and 37 °C were applied for dissolved oxygen and the temperature,
145 respectively [39, 40]. The culture was continuously stirred which was controlled with the adaptive my-
146 Control system. The stirrer speed increased linearly with decreasing oxygen below the setpoint up to
147 a maximum of 1200 RPM. The stirrer speed decreased linearly with increasing oxygen above the
148 setpoint down to a minimum of 220 RPM.
149 To determine kynurenine pathway metabolism of the individually grown bacteria in the bioreactor, a
150 single colony of *P. fluorescens* or 1 mL overnight grown precultures of *E. coli*, *S. salivarius*, *S.*
151 *thermophilus* or *L. casei* was added to 200 mL EBB supplemented with 500 µM tryptophan and, if
152 indicated, 100 µM kynurenine. At the start (0h) and at termination of the experiment (24h) 250 µL
153 culture was transferred to a new tube and immediately 1 mL cold (-20 °C) methanol was added. The
154 samples were stored at -20 °C until further use.
155 Community growth was obtained via inoculation of a single colony of *P. fluorescens* MFY63 in 200 mL
156 EBB supplemented with 500 µM tryptophan and, if indicated, 100 µM kynurenine. After 23 hours of

157 growth, 1 mL of combined overnight grown pre-cultures of *E. coli* (1:10000)*, S. Salivarius* (1:100) and
158 *L. casei* (1:100) or *S. thermophilus* (1:100) were added. At 0, 3, 5, 7, and 24 hours after inoculation with
159 the overnight grown pre-cultures a 5 mL sample was obtained. Immediately 250 µL was added to 400
160 µL NMR buffer (200 mM Na_2HPO_4, 44 mM NaH_2PO_4, 1 mM TSP, 3 mM NaN_3 and 20% (v/v) D_2O),
161 centrifuged at 4 °C, 21130 rcf for 20 min and 550 µL was transferred to a 5 mm NMR tube. For biomass
162 determination, 1.5 mL sample was centrifuged at room temperature for 1 min at 21130 rcf. The
163 supernatant was removed and the wet pellet was weighed. Lastly, 250 µL sample was transferred to a
164 new tube and immediately 1 mL cold (-20 °C) methanol was added. The samples were stored at -20 °C
165 until further use.
166
167 *UHPLC-UV*
168 Cell debris was removed from the sample stored at -20 °C in methanol by centrifugation at 4 °C, 21130
169 rcf for 10 min. The supernatant was transferred to a new tube and the methanol fraction was
170 evaporated using a Savant speed-vacuum dryer (SPD131, Fisher Scientific, Landsmeer, The
171 Netherlands) at 60 °C for 75 min. The dried material was reconstituted to 1 mL with 0.7% perchloric
172 acid. Samples were filtered using a 0.2 µM RC membranes (Phenomenex, Utrecht, The Netherlands)
173 and injected into the UHPLC system (Dionex UltiMate 3000 autosampler; Dionex UltiMate 3000 LPG-
174 3400SD pump, Thermo Fisher Scientific, Waltham, Massachusetts, USA). All samples were analyzed on
175 a C18 column (Kinetex 5 µm, C18 100 Å, 250 × 4.6 mm, Phenomenex, Utrecht, the Netherlands) using
176 a gradient of water/methanol with 0.1% formic acid (0 to 10 min, 95% to 80% H2O; 10 to 20 min, 80%
177 to 5% H2O; 20 to 23 min, 5% H2O; 23 to 31 min, 95% H2O), with a flowrate of 1 mL/min. The column
178 was kept at a temperature of 35 °C. UV-detection at 260 nm was performed with an UV6000LP
179 Detector (Dionex Ultimate 3000 variable wavelength detector, Thermo Fisher Scientific, Waltham,
180 Massachusetts, USA) Data recording and analysis were performed using Chromeleon software (version
181 6.8 SR13).
182

183 *DNA extraction*

184 DNA extraction was performed as previously described [41] from the cell pellets obtained by
185 centrifuging 1.5 mL culture for 1 min at 21130 rcf. The supernatant was removed, the pellets were
186 resuspended in 750 mL lysis buffer (500 mM NaCl, 50 mM Tris-HCl (pH 8.0), 50 mM EDTA, 4 % SDS)
187 and transferred to a 2 mL screw cap tube containing 0.5 g, 0.1 mm zirconia beads and 4, 3 mm glass
188 beads. The cells were disrupted with a mini-bead beater (3X 1 min, with 1 min intervals on ice) and
189 incubated at 95 °C for 15 min. Cell debris was removed by centrifugation at 4 °C, 21130 rcf for 20 min.
190 500 µL of the supernatant was transferred to a clean tube. 200 µL 10 M ammonium acetate was added,
191 and the samples were incubated for 10 min on ice. The samples were centrifuged at 4 °C, 21130 rcf for
192 10 min. 600 µL was transferred to a clean tube and 600 µL isopropanol was added. The samples were
193 incubated overnight at -20 °C and afterwards centrifuged at 4 °C, 21130 rcf for 15 min to pellet the
194 nucleic acids. The supernatant was removed and to wash the nucleic acid pellet 700 µL 70 % ethanol
195 was added, the samples were mixed thoroughly and centrifuged at room temperature, 21130 rcf for 5
196 min. The pellets were completely dried by leaving the tubes open for 60 min at room temperature and
197 were dissolved in 100 µL MilliQ.

198

199 *Digital chip-based PCR analysis*

200 Chip-based digital polymerase chain reaction (c-dPCR) was performed with the QuantStudio™ 3D
201 Digital PCR System (User Guide, Catalog Number A29154, Thermo Scientific). Each c-dPCR reaction was
202 prepared in a final volume of 15,5 µL containing 5 µL QuantStudio™ 3D Digital PCR Master Mix v2
203 (Applied Biosystems), 1 µM end concentration forward and reverse primer, 0,25 µM end concentration
204 probe **(Supplementary table 1, Eurogentec)** and nuclease free water. 1 µL extracted genomic DNA was
205 added to the reaction mix. The DNA concentration was estimated by using the cycle threshold values
206 from the qPCR run. For no-template control 1 µL nuclease free water was added instead of genomic
207 DNA. The positive control was extracted genomic DNA from pure cultures. 14,5 µL was loaded into the
208 QuantStudio™ 3D Digital 20K Chip v2 using the QuantStudio™ 3D Digital PCR Chip Loader. The

209 amplification reactions were performed in the QuantStudio™ 3D Digital PCR System. The PCR
210 conditions were: 10 minutes at 96 °C for DNA polymerase activation, followed by 40 two-step cycles
211 of 2 minutes at 60 °C, 30 seconds at 98 °C and a final extension for 2 minutes at 60 °C and an infinite
212 10°C hold until the chips were read. After DNA amplification the chips were transferred to the
213 QuantStudio™ 3D Digital PCR Chip reader for imaging. The end-point fluorescence data were collected
214 and analyzed using the QuantStudio™ 3D AnalysisSuite cloud software (version 3.1.6-PRC-build18).
215 Droplets were considered positive when the fluorescence signal was above the threshold. The
216 threshold was set to the positive control DNA and no-template control. The number of positive and
217 negative reactions were counted and using Poisson statistics to measure absolute copies per µL.
218
219 *^{1}H NMR spectroscopy and data processing*
220 All ^{1}H-NMR spectra were recorded using a Bruker 600 MHz AVANCE II spectrometer equipped with a
221 5 mm triple resonance inverse cryoprobe and a z-gradient system. The temperature of the samples
222 was maintained at 25 °C during measurement. Prior to data acquisition, tuning and matching of the
223 probe head followed by shimming and proton pulse calibration were performed automatically for each
224 sample. One-dimensional (1D) ^{1}H-NMR spectra were recorded using the first increment of a NOESY
225 pulse sequence with presaturation (γB_1 = 50 Hz) for water suppression during a relaxation delay of 4 s
226 and a mixing time of 10 ms. 256 scans of 65,536 points covering 13,658 Hz were recorded and zero
227 filled to 65,536 complex points prior to Fourier transformation, an exponential window function was
228 applied with a line-broadening factor of 1.0 Hz. The spectra were phase and baseline corrected and
229 referenced to the internal standard (TSP; δ 0.0 ppm), using the MestReNova software (v.12.0.0-20080,
230 Mesterlab Research). With the same software, spectral alignment was performed selecting manually
231 areas and applying a linear filling method of the missing values, after the exclusion of the water signal
232 and the surrounding empty area (4.50-5.30 ppm). Spectral binning followed from -0.50 to 9.00 ppm
233 with an equal size binning step of 0.005 ppm. Noise removal was performed by averaging each
234 integrated bin separately and removing the bins with an average below 100. Before ordination analysis

235 bins belonging to TSP (-0.50 – 0.72 ppm), ethanol (1.170 – 1.220 ppm and 3.640 – 3.690 ppm) and a
236 pH sensitive area (7.850 – 8.190 ppm) were removed. The annotation of the bins was performed with
237 the Chenomx Profiler software (Chenomx NMR Suite 8.6 and Chenomx 600 MHz, version 11) and the
238 HMDB database 5.0 (http://www.hmdb.ca).
239
240 *Statistical and network analysis*
241 All analysis of variance (ANOVA) were performed using GraphPad Prism 7.0. When a comparison
242 resulted in a statistically significant difference ($P < 0.05$), multiple comparisons testing was performed
243 by controlling the false discovery rate (FDR) according to the Benjamini-Hochberg method ($\alpha < 0.05$).
244 The R package MixOmics was used for ordination and multivariate statistical analysis of the ^{1}H-NMR
245 spectra [42]. The dynamic profile comparison using Kendall's τ correlation with the BH ($\alpha < 0.05$) was
246 performed using the R package psych. In CytoScape 3.9.1 the plugin CoNet [43] was used for network
247 construction. The network properties were obtained using the network analyzer tool. To analyze the
248 PLS-DA separation, the accuracy, R2, Q2 and *P*-value of a permutation test performed with the
249 separation distance statistic and 1000 permutations are calculated using MetaboAnalyst 5.0 [44].
250
251 **Results**
252 *Kynurenine pathway metabolism and pH changes in a three species synthetic community*
253 To investigate the metabolic network changes resulting from probiotic supplementation, it is critical
254 to carefully select bacterial members for the community. These members should be isolated from the
255 normal small intestinal microbiota and capable of metabolizing key proximal small intestinal
256 metabolites such as, acetate and lactate [7]. Additionally, the kynurenine pathway should be affected
257 by the community. In this study, *Streptococcus salivarius* and two bacteria capable of affecting the
258 kynurenine pathway, namely *Pseudomonas fluorescens* and *Escherichia coli* [33, 45–47], were selected.
259 Two commonly used probiotic species, which were previously shown to be active in the small intestine,
260 *Streptococcus thermophilus* W69 [48, 49] and *Lactobacillus casei* W56 [50], were added separately to

261 distinguish between general and species-specific effects of probiotic supplementation. Before
262 constructing the community, each species was separately grown in flasks with 500 µM tryptophan and
263 kynurenine or KYNA to investigate the ability of the various community strains to metabolize
264 kynurenine pathway metabolites. After 24 hours of incubation, kynurenine pathway metabolism was
265 observed for *P. fluorescens* and *E. coli*, but not for *S. salivarius*, *S. thermophilus* and *L. casei*
266 **(Supplementary figure 1)**. To confirm the kynurenine pathway metabolism in conditions resembling
267 the upper small intestine, each strain is separately grown in a MiniBio 250 mL bioreactor
268 (Applikon Biotechnology, The Netherlands) at 37 °C with controlled pO2 (50% of the atmospheric air)
269 as previously described [39, 40] with and without 100 µM kynurenine. After 24 hours of incubation,
270 the results revealed that *E. coli* effectively metabolized tryptophan and converted kynurenine into
271 KYNA. Conversely, *P. fluorescens* produced only a small amount of kynurenine from tryptophan. In
272 contrast, *S. salivarius*, *S. thermophilus*, and *L. casei* did not metabolize either tryptophan or kynurenine
273 **(Supplementary figure 2A)**. These findings confirm the differential metabolic capabilities of bacterial
274 species in relation to kynurenine pathway metabolism. Concurrently, the pH dynamics of each strain
275 cultured in the presence or absence of kynurenine were assessed. *P. fluorescens* did not exhibit any
276 noticeably pH changes during the course of the experiment, whereas *E. coli*, *S. salivarius* and *S.*
277 *thermophilus* demonstrated a decrease in pH after 3.5h of growth. *L. casei* reduced the pH after 12h
278 of growth. Among all bacteria, only *E. coli* displayed an increase in pH after 6h. Comparable pH profiles
279 were observed for all bacteria, except for *E. coli* when incubated with 100 µM kynurenine. Co-culturing
280 *E. coli* with kynurenine resulted in an earlier and more pronounced decline in pH **(Supplementary**
281 **figure 2B)**.
282 The synthetic community was then grown in the bioreactor under the same conditions stated above.
283 *P. fluorescens* was initially cultured in the bioreactor for a period of 23h. Thereafter, *S. salivarius*, *E.*
284 *coli* and one of the probiotic species were added to the bioreactor to create a bacterial community.
285 Furthermore, we supplemented each community with 100 µM kynurenine to simulate increased
286 activity of the small intestinal kynurenine pathway. The small intestine is known to undergo rapid

287 changes in response to food ingestion, necessitating the need for the bacterial community to adapt
288 [16, 51]. Moreover, substantial metabolism was observed in individually grown bacteria after 3.5h of
289 growth, as indicated by the pH profile **(Supplementary figure 2B).** Therefore, we collected samples
290 from the community at 0, 3, 5, 7 and 24h after community growth and analyzed the biomass, absolute
291 species distribution using c-dPCR, metabolic environment using ^{1}H-NMR, and kynurenine metabolism
292 using HPLC-UV **(Figure 1A)**. Our results showed that both kynurenine (between 3 and 7h) and KYNA
293 (between 7 and 24h) were produced in the control and probiotic-supplemented communities, with
294 kynurenine addition increasing KYNA production in all communities **(Supplementary figure 3)**.
295 However, we observed that the addition of kynurenine together with *L. casei* increased the levels of
296 kynurenine after 5h of growth when compared to the control and *S. thermophilus* supplemented
297 community in the presence of kynurenine and after 7h of growth only in the *S. thermophilus*
298 supplemented community in the presence of kynurenine subsequently leading to increased levels of
299 KYNA after 7 and 24h of growth compared to the control and *S. thermophilus* supplemented
300 communities **(Figure 1B)**. Moreover, the pH declined sharply after 3h of community growth, followed
301 by a linear increase and a plateau after 10h of growth **(Figure 1C)**, and the addition of kynurenine did
302 not affect the lowest pH and the time it was reached (ordinary two-way ANOVA; $F(1,12) = 1.78$, $P =$
303 0.21 and $F(1,12) = 0.76$, $P = 0.4$ respectively) **(Table 1)**. Probiotic supplementation altered both the
304 lowest pH and the time it was reached (ordinary two-way ANOVA; $F(2,12) = 6.85$, $P = 0.01$ and $F(2,12)$
305 $= 4.0$, $P = 0.047$) **(Table 1)**, mostly attributed to differences between *L. casei* and *S. thermophilus*
306 supplementation **(Figure 1C, Supplementary figure 4)**, indicating a probiotic specific effect.
307 Overall, the addition of kynurenine together with *L. casei* increased the production of kynurenine and
308 subsequently KYNA compared to the control and *S. thermophilus* supplemented communities.
309 Probiotic supplementation altered both the lowest pH and the time it was reached, mostly attributed
310 to differences between *L. casei* and *S. thermophilus* supplementation, indicating a probiotic-specific
311 effect. These findings suggest that probiotics, particularly *L. casei*, may influence the production of

312 kynurenine pathway metabolites in the small intestine, which could have important implications for
313 human health.
314
315 *Effect of kynurenine and probiotic supplementation on biomass and cell counts in a simplified bacterial*
316 *community*
317 Bacteria can gain a competitive advantage in a community through metabolizing compounds present
318 in the environment, inhibiting the growth of competitors, or stimulating other bacteria to secrete
319 beneficial metabolites [52]. Therefore, we hypothesized that the supplementation of a probiotic
320 species or kynurenine, which was only metabolized by *P. fluorescens* and *E. coli* **(Supplementary figure**
321 **2A)**, may alter the composition of the simplified community. The total biomass and the community
322 composition were compared **(Figure 1A)** to investigate the effects of kynurenine and probiotic
323 supplementation on community growth. Kynurenine addition did not affect the biomass, while
324 probiotic addition altered total biomass production after 7h of growth **(Supplementary data 1).**
325 Specifically, the addition of *L. casei* resulted in an increase in biomass in the absence of kynurenine,
326 while the introduction of *S. thermophilus* in the presence of kynurenine led to a reduction in the total
327 biomass **(Supplementary figure 5)**.
328 Next, the total cell count and cell count of specific species in the community were monitored using c-
329 dPCR. Kynurenine supplementation did not affect the total cell count or the cell count of any individual
330 species **(Supplementary data 2).** Furthermore, probiotic supplementation did not alter the cell count
331 of *P. fluorescens* **(Figure 2, Supplementary data 2)**, but probiotic supplementation altered the total
332 cell count and the cell count of *E. coli* (after 3 and 5h of growth, although multiple comparison testing
333 did not identify specific alterations), and of *S. salivarius* (after 5 and 7h of growth) **(Figure 2,**
334 **supplementary data 2)**, which coincides with the decrease in pH **(Figure 1C)** and with the growth of *S.*
335 *thermophilus* **(Figure 2).** In contrast, the cell counts of *L. casei* continuously increased over time **(Figure**
336 **2)**. Cell counts of the probiotic species were not affected by kynurenine supplementation at any
337 sampling point **(Figure 2)**. Specifically, *L. casei* addition inhibited the growth of *S. salivarius* by altering

338 the community metabolism. These results suggest that the supplementation of certain compounds,
339 exemplified here by kynurenine, or probiotics, or a combination of both, can alter the growth and
340 composition of bacterial communities, which could have implications for the design of probiotic
341 therapies.
342
343 *Metabolic network analysis of probiotic supplementation and kynurenine metabolism in the synthetic*
344 *bacterial community.*
345 In order to elucidate the metabolic changes that are associated with alterations in pH, kynurenine
346 metabolism and cell count, we employed ^{1}H-NMR to analyze the supernatant **(Figure 1A).** Following
347 spectral binning and processing, a total of 943 bins were subjected to principal component analysis
348 (PCA). Our results revealed time-dependent clustering of the samples **(Figure 3A)**, whereby the most
349 significant contributors to the observed separation were lactate (bin 366, 368 and 369), acetate (bin
350 485 and 486).
351 To determine whether the dynamic metabolic profiles of the community were altered by probiotic or
352 kynurenine supplementation, we conducted partial least squares – discriminant analysis (PLS-DA) with
353 cross validation (CV) and a permutation test was performed with the 943 bins as input. Our analysis
354 revealed no significant differentiation between communities with and without kynurenine
355 supplementation, nor between control and *S. thermophilus*-supplemented communities
356 **(Supplementary figure 6A and 6B)**. However, we observed significant separation in communities
357 supplemented with *L. casei,* with lactate (bin 923), glucose (bin 851 and 853) and threonine (bin 820)
358 contributing most to the separation from the control **(Figure 3B)**. Additionally, glucose (bin 848, 851
359 and 853 – 856), glycerol (bin 815) and cadaverine (bin 707) were the major contributors to the
360 differentiation between *L. casei* and *S. thermophilus* supplemented communities **(Figure 3C)**.
361 To demonstrate the metabolic contributions responsible for the variance obtained from the entire
362 spectral dataset, the chemical library of Chenomx profiler software and the online human metabolome
363 database version 5.0 were utilized. We identified 30 metabolites, and subjected the area under the

364 curve (AUC) of a representative peak for each metabolite to ordination analysis. The results of this
365 approach were similar to the ordination analyses conducted with the bins. PCA revealed temporal
366 clustering of the samples and PLS-DA revealed significant separation of the *L. casei* supplemented
367 community from the control and *S. thermophilus* supplemented communities **(Supplementary figure**
368 **7A, B and C)**. Therefore, we postulated that the AUC values of the identified set of metabolites may
369 serve as a surrogate for the full spectra dataset and could be employed for subsequent analysis.
370 Given that the metabolic network of a community is highly interconnected, a substantial alteration in
371 certain metabolites can lead to multiple smaller changes in related metabolites that might not be
372 detectable by ordination analysis **(Figure 3A, B and C)**. Similarly, minor effects of kynurenine
373 supplementation on metabolism may go undetected via ordination analysis. To investigate smaller
374 metabolic changes induced by kynurenine or probiotic addition to the synthetic community, we
375 compared the dynamic metabolic profiles between experiments, which revealed similarities
376 **(Supplementary figure 8)** and differences in the dynamics of saccharolytic and proteolytic community
377 metabolism **(Figure 3D, Supplementary data 3)**. Of note, we observed increased lactate production in
378 the *S. thermophilus* supplemented community, which could potentially account for the observed pH
379 variation **(Figure 1C)**.
380 To explore the coordinate behavior of metabolites and network topology features across the tested
381 conditions [53], we constructed dynamic correlation-based networks using the Cytoscape plugin CoNet
382 [43], whereby the nodes represent the metabolites and the edges represent correlations between the
383 metabolic profiles per condition. Without kynurenine, *S. thermophilus* supplementation decreased the
384 number of edges and the clustering coefficient, while the metabolite with the highest number of edges
385 was aspartate (7), compared to cadaverine (12) in the control network **(Figure 3E, table 2)**. *L. casei*
386 supplementation had a more drastic effect on the network, increasing the number of edges, clustering
387 coefficient and network density substantially **(Figure 3E, table 2)**. Kynurenine supplementation
388 reduced the number of edges, including indole, present in the control community network, and
389 reduced the number of edges of cadaverine from 12 to 1. Consequently, cadaverine and indole no

390 longer connected two major hubs of connected metabolites compared to control community. The
391 clustering coefficient and network density of the control community supplemented with kynurenine
392 was 1, due to the connections between all the metabolites with all the other metabolites in each hub
393 **(Figure 3E, table 2)**. Kynurenine supplementation to the *S. thermophilus* and *L. casei* supplemented
394 communities increased the number of edges, clustering coefficient and network density, with indole
395 and cadaverine being the metabolites with the most edges, similar to the control network without
396 kynurenine supplementation **(Figure 3E, table 2).** The node degree and betweenness centrality of
397 individual metabolites were also analyzed, showing probiotic-specific effects on the community
398 metabolism as well as an effect of kynurenine supplementation on cadaverine metabolism
399 **(Supplementary data 4)**. Together the network analysis revealed probiotic-specific effects on the
400 community metabolism and an effect of kynurenine supplementation on clustering coefficient,
401 network density and node parameters of the metabolic networks, mainly due to alterations in
402 cadaverine utilization.
403
404 **Discussion**
405 The present study investigated the impact of probiotic supplementation on metabolism of the small
406 intestinal microbiota. To achieve this, we constructed a synthetic community consisting of three gut
407 isolates that mimicked the microbial community of the upper small intestine. Specifically, we examined
408 the metabolic impact of probiotic supplementation on both general metabolism and the kynurenine
409 pathway, which has been implicated in the modulation of immune responses and neuroinflammation.
410 Our findings shed light on the probiotic-specific mechanisms of action that drive colonization
411 resistance in the small intestine and suggest that the kynurenine pathway may be a promising target
412 for future probiotic-based therapies aimed at promoting intestinal health.
413 Probiotics are known to exert their effects through competitive exclusion often by reducing the pH of
414 the gut milieu through increased lactate production [54]. In our study, supplementation with *S.*
415 *thermophilus* led to increased lactate production, resulting in a reduction in pH, and accompanied by

416 a decrease in formate and acetate levels **(Figure 3D and 1C)**. However, this supplementation did not
417 result in significant changes to the composition of the community **(Figure 2)** or the dynamic metabolic
418 network **(Figure 3E)**. Conversely, when *L. casei* was supplemented, we observed a reduction in the
419 growth of *S. salivarius*, which was not accompanied by increased lactate production **(Figure 2, 3D)**.
420 Other studies have also reported beneficial effects of *L. casei* supplementation independent of
421 acidification or lactate production [55]. These results suggest that *L. casei* supplementation alters the
422 metabolic environment, improving metabolic utilization and thereby, possibly, enhancing the
423 resistance of the community to perturbations **(Figure 3D and E).** This finding is consistent with previous
424 studies showing a positive association between habitual *L. casei* Shirota intake and long-term
425 compositional stability of the fecal microbiota [56].
426 The concept of direct colonization resistance refers to the ability of the resident microbiota to resist
427 the colonization and expansion of invading species [57]. However, decreased diversity can lead to
428 unoccupied ecological niches that can be occupied by invading species potentially harmful to host
429 health [58]. Probiotics have been proposed as a means to increase colonization resistance by filling
430 unoccupied niches before pathogenic species can colonize [59]. However, current probiotic
431 interventions do not take into account the functional capacity of probiotics to occupy specific niches
432 in the gut [60], which may explain the variable effectiveness of probiotics [61]. To address this,
433 synthetic communities are constructed [22, 62–65], but the lack of molecular insights has hampered
434 the development of probiotic therapies. The genetic capacity of *L. casei* in our synthetic community of
435 three species made it more functionally diverse **(Figure 3D)** compared to the three initial community
436 members and compared to *S. thermophilus*, which resembles *S. salivarius*. Thus, our results suggest
437 several hypotheses on how the tested species mutually influence each other and consequently impact
438 the kynurenine pathway **(Figure 4)**. These hypotheses can be tested in future studies and potentially
439 expanded to include other species.; First, *L. casei* increased the metabolic utilization and, possibly, the
440 resistance of the community to perturbations **(Figure 3E, table 2)**, by occupying an empty ecological
441 niche, whereas *S. thermophilus* had to compete for the ecological niche occupied by *S. salivarius.*

442 However, the ability to occupy a niche is determined by the functional capability [66] and the
443 environment [67]. Therefore, selecting probiotic strains with a wide range of functional capacities and
444 constructing a diverse multispecies probiotic formula could be a promising approach for developing
445 effective probiotic therapies [18, 68].
446 Indirect colonization resistance involves improving the gut epithelial barrier or enhancing the hosts
447 immune system [68]. Metabolites produced by the microbiota can interact with the host and improve
448 gut integrity. For example, stimulation of GPR35 by KYNA was shown to enhance mucosal repair and
449 stimulate mucus secretion, which increased the integrity of the gut epithelial barrier [69, 70]. Thus,
450 increasing microbial production of KYNA in the small intestine may indirectly increase colonization
451 resistance. Although no in vivo studies were conducted in our study to confirm improved intestinal
452 barrier integrity due to increased microbial KYNA production resulting from probiotic addition, we
453 show that in the *L. casei* supplemented community, *E. coli* had a reduced impact on the metabolic
454 environment since the node degree and betweenness centrality of the *E. coli* produced metabolites
455 cadaverine [71] and indole [72] were lower **(Figure 3E)**. In the kynurenine and *S.*
456 *thermophilus* supplemented community, *E. coli* had an increased impact on the metabolic
457 environment **(Figure 3E),** even though this effect was not translated into increased cell counts for *E.*
458 *coli* **(Figure 2)**.
459 Overall, the present study demonstrates that supplementation with different probiotics can lead to
460 distinct alterations in the metabolic environment of the microbiota community, with *L. casei* showing
461 improved metabolic utilization. These findings highlight the importance of selecting probiotic species
462 with diverse genetic capabilities that complement the functional capacity of the resident microbiota
463 or constructing a multispecies formula. Such an approach holds promise for the development of
464 effective probiotic therapies. It emphasizes the need to consider the functional capacity of probiotic
465 species when designing interventions. Furthermore, while the probiotic species may not have directly
466 impacted the kynurenine pathway, they still had an influence on the metabolic profiles through
467 interactions with other species. This highlights the importance for researchers to consider not only the

468 direct effects of probiotic species but also their impacts on the overall community metabolism.
469 Moreover, the present findings suggest that increasing microbial production of metabolites such as
470 KYNA in the small intestine may indirectly improve intestinal barrier integrity and increase colonization
471 resistance. Further in vivo studies are necessary to confirm the effects of probiotic supplementation
472 on intestinal barrier integrity and to develop probiotic therapies aimed at specific ecological niches in
473 the gut.
474
475 **Author Contributions:** JJ, SEA: Conceptualization, investigation, writing-original draft, and editing; JJ,
476 ACC, KC: data analysis; JJ, ACC: methodology; SvH: Conceptualization, writing review; SEA: funding
477 acquisition. All authors have read and agreed to the published version of the manuscript.
478 **Acknowledgements:** We thank Valeria Mathlener of Winclove, B.V. assisting us with the c-dPCR
479 measurements.
480 **Conflicts of Interest:** S. van Hemert is employee in Winclove (Winclove manufactures and markets
481 probiotics). The content of this study was neither influenced nor constrained by this fact. The other
482 authors have no conflicts of interest to declare.
483 **Funding:** SEA has received research funding support from Winclove, B.V. This support neither
484 influenced nor constrained the contents of this article
485 **Data availability:** The raw ^{1}H-NMR data was deposited in the Metabolights public repository [73] under
486 the accession number: MTBLS7370
487
488
489
490
491
492
493

494

495 **Tables**

496 **Table 1: properties of the pH profile of each community**.

497 The mean ± SD of the lowest pH value and time the lowest pH value was reached for all communities

498 with and without kynurenine (kyn) supplementation.

Communities	Lowest pH value	Time of the lowest pH value (h)
Control	5.69 ± 0.09	4.7 ± 0.2
S. thermophilus	5.56 ± 0.08	3.8 ± 0.1
L. casei	5.77 ± 0.03	4.5 ± 0.7
Control + kyn	5.77 ± 0.17	4.0 ± 0.2
***S. thermophilus* + kyn**	5.53 ± 0.11	3.9 ± 0.3
***L. casei* + kyn**	6.05 ± 0.25	4.6 ± 0.4

499

500

501

502

503

504

505

506

507

508

509

510

511

512

513

514

515

516

517

518 **Table 2: Properties of the dynamic correlation-based metabolic networks for each community**. The

519 number of nodes, edges, clustering coefficient, network density and the nodes with the most edges of

520 the networks depicted in figure 3E for the communities with probiotic or kynurenine (kyn)

521 supplementation.

Communities	Nodes	Edges	Clustering coefficient	Network density	Node with the most edges (edges)
Control	24	54	0.857	0.368	Cadaverine (12)
S. thermophilus	23	40	0.794	0.374	Aspartate (7)
L. casei	17	94	0.935	0.886	Gluconolactone/gluconate, glycerol (14)
***L. casei* + kyn**	24	103	0.892	0.654	Glucose, tryptophan, glycerol (16)
***S. thermophilus* + kyn**	20	56	0.901	0.549	Indole, cadaverine (12)
Control + kyn	20	54	1	1	Tryptophan, phenylalanine, alanine, methionine, glutamate, proline, isoleucine, glycine, valine, tyrosine (9)

522

523

524

525

526

527

528

529

530

531

532

533

534

535

536

537

538

539 **Figure legends**

540 **Figure 1: *Lactobacillus casei* supplementation increases kynurenine pathway metabolism in a**
541 **synthetic community**

542 A) Overview of the construction of the community and sampling procedure. *P. fluorescens* was
543 inoculated 23h prior to inoculating other species with probiotics. PH and pO_2 (indicated with dashed
544 line) were continuously measured. Black arrows indicate sampling points (0, 3, 5, 7 and 24h) for
545 obtaining metabolomics, compositional and biomass data. All experiments were performed in
546 triplicates. B) Boxplots showing the area under the curve (AUC) for kynurenine and kynurenic acid as
547 measured from the HPLC-UV chromatograms normalized to the AUC of the initial tryptophan peak
548 obtained from -23h. Significant comparisons are depicted with letters (a-d): a: $q < 0.05$, b: $q < 0.01$, c:
549 $q < 0.001$ and d: $q < 0.0001$ as obtained with an ordinary two-way ANOVA and multiple comparisons
550 testing by controlling the false discovery rate according to the Benjamini-Hochberg procedure. C) pH
551 profile for control, *S. thermophilus* supplemented and *L. casei* supplemented communities
552 with/without kynurenine. Sampling points indicated by dashed lines. Boxplot indicates the lowest pH
553 value per condition. Significant differences are indicated with asterisks; *, $q < 0.05$, as obtained with
554 an ordinary one-way ANOVA and multiple comparison testing by controlling the false discovery rate
555 according to the Benjamini-Hochberg procedure.

556

557 **Figure 2: Supplementation of *Lactobacillus casei* reduces the growth of *Streptococcus salivarius* in a**
558 **simplified community**

559 Boxplots of total cell count and cell count per species of a simplified community (*E. coli*, *S. salivarius*
560 and *P. fluorescens*) determined after 3, 5, 7 and 24h of growth. Cell counts of the communities grown
561 with the supplemented probiotic species *L. casei* or *S. thermophilus* are depicted in different colors.
562 Control or probiotic supplemented communities grown with 100 µM kynurenine are shown with
563 stripes. Statistical differences between communities were determined by ordinary two way ANOVA

approach per timepoint, and significant differences ($q < 0.05$) after multiple comparisons testing by controlling the false discovery rate according to the Benjamini-Hochberg procedure are indicated with asterisks. Probiotic addition altered the cell count of *E. coli* after 3 and 5h of growth, and the cell count of *S. salivarius* after 7h of growth (ordinary two-way ANOVA: $F(2,12) = 4.43$ and $P = 0.036$, $F(2,12) = 4.15$, $P = 0.043$ and $F(2,12) = 7.62$, $P = 0.007$ respectively), but multiple comparisons testing did not yield any significant differences. Cell counts of added probiotic species grown with and without kynurenine per timepoint were compared by performing an unpaired t test.

Figure 3: Probiotic and kynurenine supplementation alter the metabolism of a simplified community in a specific manner

A) PCA with binned ^{1}H-NMR spectra as input showing separation of metabolites with lactate (bin 366,368 and 369), acetate (bin 485 and 486) being the most distinguishing factors (indicated with arrows). The ellipses represent the 95 % confidence interval. B) PLS-DA with binned ^{1}H-NMR spectra of control and *L. casei* supplemented communities, indicating lactate (bin 923), glucose (bin 851 and 853), and threonine (bin 820) as contributing factors. C) PLS-DA with binned ^{1}H-NMR spectra of *S. thermophilus* and *L. casei* supplemented communities indicating glucose (bin 848, 851 and 853 – 856), glycerol, (bin 815) and cadaverine (bin 707) as contributing factors. Statistical parameter accuracy, R2 and Q2 and *P*-values are included. The *P*-value is the results of a permutation test performed with the separation distance statistic and 1000 permutations. All parameters were calculated using MetaboAnalyst 5.0. D) Dynamic profiles of the significantly different saccharolytic and proteolytic metabolites with repeated measure two-way ANOVA showing significant differences. The error bars indicate the standard deviation. The timepoints where a significant result of multiple comparison testing by controlling the false discovery rate according to the Benjamini-Hochberg procedure is obtained are indicated with an asterisk; *: $q < 0.05$, detailed results of the multiple comparison tests can be found in the supplementary data 3. E) Dynamic correlation-based networks of all measured metabolites in the communities showing positive and negative correlations via red solid and blue dashed edges, respectively. Nodes represent metabolites. Edges represents correlations between the

590 two connected nodes, obtained when 2/3 methods give a positive results; Kendall's $-0.9 > \tau > 0.9$,
591 Spearman's $-0.9 > \rho > 0.9$. Brown's randomization method with 1000 iterations had a Benjamini-
592 Hochberg corrected *P*-value < 0.05. The calculation of the edges was performed using the Cytoscape
593 plugin CoNet.

594 **Figure 4: Possible hypotheses of how our tested species affect each other and thereby the**
595 **kynurenine pathway**. A) Microbial community composed of *P. fluorescens*, *E. coli*, and *S. salivarius* can
596 metabolize certain metabolites present in their shared metabolic environment (depicted in squares),
597 while being unable to metabolize others (depicted in stars). If an invading pathogen can metabolize
598 the unused metabolites, it may colonize and produce metabolites with a negative impact on host
599 health (depicted in pentagons). Probiotic intervention may prevent the colonization of invading
600 pathogens, but only if the functional profile of the probiotic species complements the functional
601 capacity of the existing microbiota. In our tested species, B) *S. thermophilus* is functionally similar to *S.*
602 *salivarius*; thus, the invading pathogen would still be able to colonize and negatively affect host health.
603 On the contrary, C) *L. casei* is functionally different from the existing microbiota and can metabolize
604 the unused metabolites (stars) into metabolites that the existing microbiota can utilize. As a result, an
605 invading pathogen cannot occupy the ecological niche, preventing colonization and positively affecting
606 host health. Additionally, the increased production of metabolites by *L. casei* enhances the metabolism
607 of the existing microbiota, consequently increasing the cross-feeding reaction between *P. fluorescens*
608 and *E. coli* regarding the kynurenine pathway, which positively affects the host as well.

609

610 **References**

611 1. Hou K, Wu ZX, Chen XY, Wang JQ, Zhang D, Xiao C, et al. Microbiota in health and diseases.
612 *Signal Transduction and Targeted Therapy 2022 7:1* 2022; **7**: 1–28.
613 2. de Vos WM, Tilg H, van Hul M, Cani PD. Gut microbiome and health: mechanistic insights. *Gut*
614 2022; **71**: 1020–1032.
615 3. Donaldson GP, Lee SM, Mazmanian SK. Gut biogeography of the bacterial microbiota. *Nat Rev*
616 *Microbiol* 2016; **14**: 20.
617 4. Leite G, Morales W, Weitsman S, Celly S, Parodi G, Mathur R, et al. The duodenal microbiome
618 is altered in small intestinal bacterial overgrowth. *PLoS One* 2020; **15**: e0234906.
619 5. Villmones HC, Svanevik M, Ulvestad E, Stenstad T, Anthonisen IL, Nygaard RM, et al.
620 Investigating the human jejunal microbiota. *Sci Rep* 2022; **12**.

621 6. Roberti MP, Rauber C, Kroemer G, Zitvogel L. Impact of the ileal microbiota on colon cancer.
622 *Semin Cancer Biol* 2022; **86**: 955–966.
623 7. Zoetendal EG, Raes J, Van Den Bogert B, Arumugam M, Booijink CC, Troost FJ, et al. The
624 human small intestinal microbiota is driven by rapid uptake and conversion of simple
625 carbohydrates. *The ISME Journal 2012 6:7* 2012; **6**: 1415–1426.
626 8. Kaczmarczyk M, Löber U, Adamek K, Węgrzyn D, Skonieczna-Żydecka K, Malinowski D, et al.
627 The gut microbiota is associated with the small intestinal paracellular permeability and the
628 development of the immune system in healthy children during the first two years of life.
629 *Journal of Translational Medicine 2021 19:1* 2021; **19**: 1–26.
630 9. Martinez-Guryn K, Hubert N, Frazier K, Urlass S, Musch MW, Ojeda P, et al. Small intestine
631 microbiota regulate host digestive and absorptive adaptive responses to dietary lipids. *Cell*
632 *Host Microbe* 2018; **23**: 458.
633 10. Roberti MP, Rauber C, Kroemer G, Zitvogel L. Impact of the ileal microbiota on colon cancer.
634 *Semin Cancer Biol* 2022; **86**: 955–966.
635 11. Nouvenne A, Ticinesi A, Tana C, Prati B, Catania P, Miraglia C, et al. Digestive disorders and
636 Intestinal microbiota. *Acta Bio Medica : Atenei Parmensis* 2018; **89**: 47.
637 12. Wong AC, Levy M. New Approaches to Microbiome-Based Therapies. *mSystems* 2019; **4**.
638 13. Hill C, Guarner F, Reid G, Gibson GR, Merenstein DJ, Pot B, et al. The International Scientific
639 Association for Probiotics and Prebiotics consensus statement on the scope and appropriate
640 use of the term probiotic. *Nature Reviews Gastroenterology & Hepatology 2014 11:8* 2014;
641 **11**: 506–514.
642 14. Barbosa SJ de A, Oliveira MMB, Ribeiro SB, de Medeiros CACX, Lima ML de S, Guerra GCB, et
643 al. The beneficial effects of Lacticaseibacillus casei on the small intestine and colon of Swiss
644 mice against the deleterious effects of 5-fluorouracil. *Front Immunol* 2022; **13**: 6411.
645 15. Zhong C, Qu C, Wang B, Liang S, Zeng B. Probiotics for Preventing and Treating Small Intestinal
646 Bacterial Overgrowth. *J Clin Gastroenterol* 2017; **51**: 300–311.
647 16. Yilmaz B, Fuhrer T, Morgenthaler D, Krupka N, Wang D, Spari D, et al. Plasticity of the adult
648 human small intestinal stoma microbiota. *Cell Host Microbe* 2022; **30**: 1773-1787.e6.
649 17. Colom J, Freitas D, Simon A, Brodkorb A, Buckley M, Deaton J, et al. Presence and
650 Germination of the Probiotic Bacillus subtilis DE111® in the Human Small Intestinal Tract: A
651 Randomized, Crossover, Double-Blind, and Placebo-Controlled Study. *Front Microbiol* 2021;
652 **12**: 2189.
653 18. Jansma J, Thome NU, Schwalbe M, Chatziioannou AC, Elsayed SS, Wezel GP van, et al.
654 Probiotics supplementation to adult human small intestinal stoma microbiota causes dynamic
655 increase in the community resistance to perturbations and nutrient utilization. *bioRxiv* 2023;
656 2023.01.29.525861.
657 19. Weiss AS, Burrichter AG, Durai Raj AC, von Strempel A, Meng C, Kleigrewe K, et al. In vitro
658 interaction network of a synthetic gut bacterial community. *The ISME Journal 2021 16:4* 2021;
659 **16**: 1095–1109.
660 20. Großkopf T, Soyer OS. Synthetic microbial communities. *Curr Opin Microbiol* 2014; **18**: 72–77.
661 21. Christensen BB, Haagensen JAJ, Heydorn A, Molin S. Metabolic Commensalism and
662 Competition in a Two-Species Microbial Consortium. *Appl Environ Microbiol* 2002; **68**: 2495.
663 22. Cheng AG, Ho PY, Aranda-Díaz A, Jain S, Yu FB, Meng X, et al. Design, construction, and in vivo
664 augmentation of a complex gut microbiome. *Cell* 2022; **185**: 3617-3636.e19.
665 23. Gutiérrez N, Garrido D. Species Deletions from Microbiome Consortia Reveal Key Metabolic
666 Interactions between Gut Microbes. *mSystems* 2019; **4**.
667 24. Kleerebezem M, Binda S, Bron PA, Gross G, Hill C, van Hylckama Vlieg JE, et al. Understanding
668 mode of action can drive the translational pipeline towards more reliable health benefits for
669 probiotics. *Curr Opin Biotechnol* 2019; **56**: 55–60.
670 25. Clark RL, Connors BM, Stevenson DM, Hromada SE, Hamilton JJ, Amador-Noguez D, et al.
671 Design of synthetic human gut microbiome assembly and butyrate production. *Nature*
672 *Communications 2021 12:1* 2021; **12**: 1–16.

673 26. Blasche S, Kim Y, Oliveira AP, Patil KR. Model microbial communities for ecosystems biology.
674 *Curr Opin Syst Biol* 2017; **6**: 51–57.
675 27. Tanoue T, Morita S, Plichta DR, Skelly AN, Suda W, Sugiura Y, et al. A defined commensal
676 consortium elicits CD8 T cells and anti-cancer immunity. *Nature 2019 565:7741* 2019; **565**:
677 600–605.
678 28. Savitz J, Savitz jsavitz J. The kynurenine pathway: a finger in every pie. *Molecular Psychiatry*
679 *2019 25:1* 2019; **25**: 131–147.
680 29. Laurans L, Venteclef N, Haddad Y, Chajadine M, Alzaid F, Metghalchi S, et al. Genetic
681 deficiency of indoleamine 2,3-dioxygenase promotes gut microbiota-mediated metabolic
682 health. *Nature Medicine 2018 24:8* 2018; **24**: 1113–1120.
683 30. Kaya B, Melhem H, Niess JH. GPR35 in Intestinal Diseases: From Risk Gene to Function. *Front*
684 *Immunol* 2021; **12**: 4610.
685 31. Turski MP, Turska M, Paluszkiewicz P, Parada-Turska J, Oxenkrug GF. Kynurenic Acid in the
686 Digestive System–-New Facts, New Challenges. *International Journal of Tryptophan Research*
687 2013; **6**: IJTR.S12536.
688 32. Kuc D, Zgrajka W, Parada-Turska J, Urbanik-Sypniewska T, Turski WA. Micromolar
689 concentration of kynurenic acid in rat small intestine Short Communication. *Amino Acids*
690 2008; **35**: 503–505.
691 33. Kurnasov O, Goral V, Colabroy K, Gerdes S, Anantha S, Osterman A, et al. NAD Biosynthesis:
692 Identification of the Tryptophan to Quinolinate Pathway in Bacteria. *Chem Biol* 2003; **10**:
693 1195–1204.
694 34. Więdłocha M, Marcinowicz P, Janoska-Jaździk M, Szulc A. Gut microbiota, kynurenine
695 pathway and mental disorders – Review. *Prog Neuropsychopharmacol Biol Psychiatry* 2021;
696 **106**: 110145.
697 35. Purton T, Staskova L, Lane MM, Dawson SL, West M, Firth J, et al. Prebiotic and probiotic
698 supplementation and the tryptophan-kynurenine pathway: A systematic review and meta
699 analysis. *Neurosci Biobehav Rev* 2021; **123**: 1–13.
700 36. Chapalain A, Rossignol G, Lesouhaitier O, Merieau A, Gruffaz C, Guerillon J, et al. Comparative
701 study of 7 fluorescent pseudomonad clinical isolates. *https://doi.org/101139/W07-110* 2007;
702 **54**: 19–27.
703 37. van den Bogert B, Boekhorst J, Herrmann R, Smid EJ, Zoetendal EG, Kleerebezem M.
704 Comparative Genomics Analysis of Streptococcus Isolates from the Human Small Intestine
705 Reveals their Adaptation to a Highly Dynamic Ecosystem. *PLoS One* 2013; **8**: e83418.
706 38. Waclawiková B, Bullock A, Schwalbe M, Aranzamendi C, Nelemans SA, van Dijk G, et al. Gut
707 bacteria-derived 5-hydroxyindole is a potent stimulant of intestinal motility via its action on L-
708 type calcium channels. *PLoS Biol* 2021; **19**: e3001070.
709 39. He G, Shankar RA, Chzhan M, Samouilov A, Kuppusamy P, Zweier JL. Noninvasive
710 measurement of anatomic structure and intraluminal oxygenation in the gastrointestinal tract
711 of living mice with spatial and spectral EPR imaging. *Proc Natl Acad Sci U S A* 1999; **96**: 4586.
712 40. Sheridan WG, Lowndes RH, Young HL. Intraoperative tissue oximetry in the human
713 gastrointestinal tract. *The American Journal of Surgery* 1990; **159**: 314–319.
714 41. Yu Z, Morrison M. Improved extraction of PCR-quality community DNA from digesta and fecal
715 samples. *Biotechniques* 2004; **36**: 808–812.
716 42. Rohart F, Gautier B, Singh A, Lê Cao KA. mixOmics: An R package for 'omics feature selection
717 and multiple data integration. *PLoS Comput Biol* 2017; **13**: e1005752.
718 43. Faust K, Raes J, Wilmes P, Heintz-Buschart A, Eiler A. CoNet app: inference of biological
719 association networks using Cytoscape. *F1000Research 2016 5:1519* 2016; **5**: 1519.
720 44. Xia J, Psychogios N, Young N, Wishart DS. MetaboAnalyst: A web server for metabolomic data
721 analysis and interpretation. *Nucleic Acids Res* 2009; **37**.
722 45. Bortolotti P, Hennart B, Thieffry C, Jausions G, Faure E, Grandjean T, et al. Tryptophan
723 catabolism in Pseudomonas aeruginosa and potential for inter-kingdom relationship. *BMC*
724 *Microbiol* 2016; **16**: 1–10.

46. Paulsen IT, Press CM, Ravel J, Kobayashi DY, Myers GSA, Mavrodi D v., et al. Complete genome sequence of the plant commensal Pseudomonas fluorescens Pf-5. *Nature Biotechnology 2005 23:7* 2005; **23**: 873–878.
47. Kuc D, Zgrajka W, Parada-Turska J, Urbanik-Sypniewska T, Turski WA. Micromolar concentration of kynurenic acid in rat small intestine. *Amino Acids* 2008; **35**: 503–505.
48. Martinović A, Cocuzzi R, Arioli S, Mora D. Streptococcus thermophilus: To Survive, or Not to Survive the Gastrointestinal Tract, That Is the Question! *Nutrients* 2020; **12**: 1–13.
49. Mater DDG, Drouault-Holowacz S, Oozeer R, Langella P, Anba J, Corthier G. β-Galactosidase production by Streptococcus thermophilus is higher in the small intestine than in the caecum of human-microbiota-associated mice after lactose supplementation. *British Journal of Nutrition* 2006; **96**: 177–181.
50. Timmerman HM, Niers LEM, Ridwan BU, Koning CJM, Mulder L, Akkermans LMA, et al. Design of a multispecies probiotic mixture to prevent infectious complications in critically ill patients. *Clinical Nutrition* 2007; **26**: 450–459.
51. Procházková N, Falony G, Dragsted LO, Licht TR, Raes J, Roager HM. Advancing human gut microbiota research by considering gut transit time. *Gut* 2022; **0**: gutjnl-2022-328166.
52. Fritts RK, McCully AL, McKinlay JB. Extracellular Metabolism Sets the Table for Microbial Cross-Feeding. *Microbiology and Molecular Biology Reviews* 2021; **85**.
53. Batushansky A, Matsuzaki S, Newhardt MF, West MS, Griffin TM, Humphries KM. GC-MS metabolic profiling reveals Fructose-2,6-bisphosphate regulates branched chain amino acid metabolism in the heart during fasting. *Metabolomics* 2019; **15**: 18.
54. van Zyl WF, Deane SM, Dicks LMT. Molecular insights into probiotic mechanisms of action employed against intestinal pathogenic bacteria. *Gut Microbes* 2020; **12**.
55. Panpetch W, Phuengmaung P, Cheibchalard T, Somboonna N, Leelahavanichkul A, Tumwasorn S. Lacticaseibacillus casei Strain T21 Attenuates Clostridioides difficile Infection in a Murine Model Through Reduction of Inflammation and Gut Dysbiosis With Decreased Toxin Lethality and Enhanced Mucin Production. *Front Microbiol* 2021; **12**: 3607.
56. Amamoto R, Shimamoto K, Park S, Matsumoto H, Shimizu K, Katto M, et al. Yearly changes in the composition of gut microbiota in the elderly, and the effect of lactobacilli intake on these changes. *Scientific Reports 2021 11:1* 2021; **11**: 1–14.
57. Sorbara MT, Pamer EG. Interbacterial mechanisms of colonization resistance and the strategies pathogens use to overcome them. *Mucosal Immunology 2018 12:1* 2018; **12**: 1–9.
58. Khan I, Bai Y, Zha L, Ullah N, Ullah H, Shah SRH, et al. Mechanism of the Gut Microbiota Colonization Resistance and Enteric Pathogen Infection. *Front Cell Infect Microbiol* 2021; **11**: 1273.
59. Litvak Y, Bäumler AJ. The founder hypothesis: A basis for microbiota resistance, diversity in taxa carriage, and colonization resistance against pathogens. *PLoS Pathog* 2019; **15**.
60. Zmora N, Zilberman-Schapira G, Suez J, Mor U, Dori-Bachash M, Bashiardes S, et al. Personalized Gut Mucosal Colonization Resistance to Empiric Probiotics Is Associated with Unique Host and Microbiome Features. *Cell* 2018; **174**: 1388-1405.e21.
61. Kristensen NB, Bryrup T, Allin KH, Nielsen T, Hansen TH, Pedersen O. Alterations in fecal microbiota composition by probiotic supplementation in healthy adults: A systematic review of randomized controlled trials. *Genome Med* 2016; **8**: 1–11.
62. Pereira FC, Wasmund K, Cobankovic I, Jehmlich N, Herbold CW, Lee KS, et al. Rational design of a microbial consortium of mucosal sugar utilizers reduces Clostridiodes difficile colonization. *Nature Communications 2020 11:1* 2020; **11**: 1–15.
63. Brand MW, Wannemuehler MJ, Phillips GJ, Proctor A, Overstreet AM, Jergens AE, et al. The Altered Schaedler Flora: Continued Applications of a Defined Murine Microbial Community. *ILAR J* 2015; **56**: 169–178.
64. Darnaud M, De Vadder F, Bogeat P, Boucinha L, Bulteau AL, Bunescu A, et al. A standardized gnotobiotic mouse model harboring a minimal 15-member mouse gut microbiota recapitulates SOPF/SPF phenotypes. *Nature Communications 2021 12:1* 2021; **12**: 1–21.

65. Brugiroux S, Beutler M, Pfann C, Garzetti D, Ruscheweyh HJ, Ring D, et al. Genome-guided design of a defined mouse microbiota that confers colonization resistance against Salmonella enterica serovar Typhimurium. *Nature Microbiology 2016 2:2* 2016; **2**: 1–12.
66. Aktas B, De Wolfe TJ, Safdar N, Darien BJ, Steele JL. The Impact of Lactobacillus casei on the Composition of the Cecal Microbiota and Innate Immune System Is Strain Specific. *PLoS One* 2016; **11**: e0156374.
67. Colombo M, Oliveira AEZ de, Carvalho AF de, Nero LA. Development of an alternative culture medium for the selective enumeration of Lactobacillus casei in fermented milk. *Food Microbiol* 2014; **39**: 89–95.
68. Sassone-Corsi M, Raffatellu M. No vacancy: how beneficial microbes cooperate with immunity to provide colonization resistance to pathogens. *J Immunol* 2015; **194**: 4081–4087.
69. Kaya B, Melhem H, Niess JH. GPR35 in Intestinal Diseases: From Risk Gene to Function. *Front Immunol* 2021; **12**: 4610.
70. Wang Z, Yin L, Qi Y, Zhang J, Zhu H, Tang J. Intestinal Flora-Derived Kynurenic Acid Protects Against Intestinal Damage Caused by Candida albicans Infection via Activation of Aryl Hydrocarbon Receptor. *Front Microbiol* 2022; **13**: 2554.
71. Akhova A, Nesterova L, Shumkov M, Tkachenko A. Cadaverine biosynthesis contributes to decreased Escherichia coli susceptibility to antibiotics. *Res Microbiol* 2021; **172**: 103881.
72. Piñero-Fernandez S, Chimerel C, Keyser UF, Summers DK. Indole transport across Escherichia coli membranes. *J Bacteriol* 2011; **193**: 1793–1798.
73. Haug K, Salek RM, Conesa P, Hastings J, De Matos P, Rijnbeek M, et al. MetaboLights - An open-access general-purpose repository for metabolomics studies and associated meta-data. *Nucleic Acids Res* 2013; **41**.

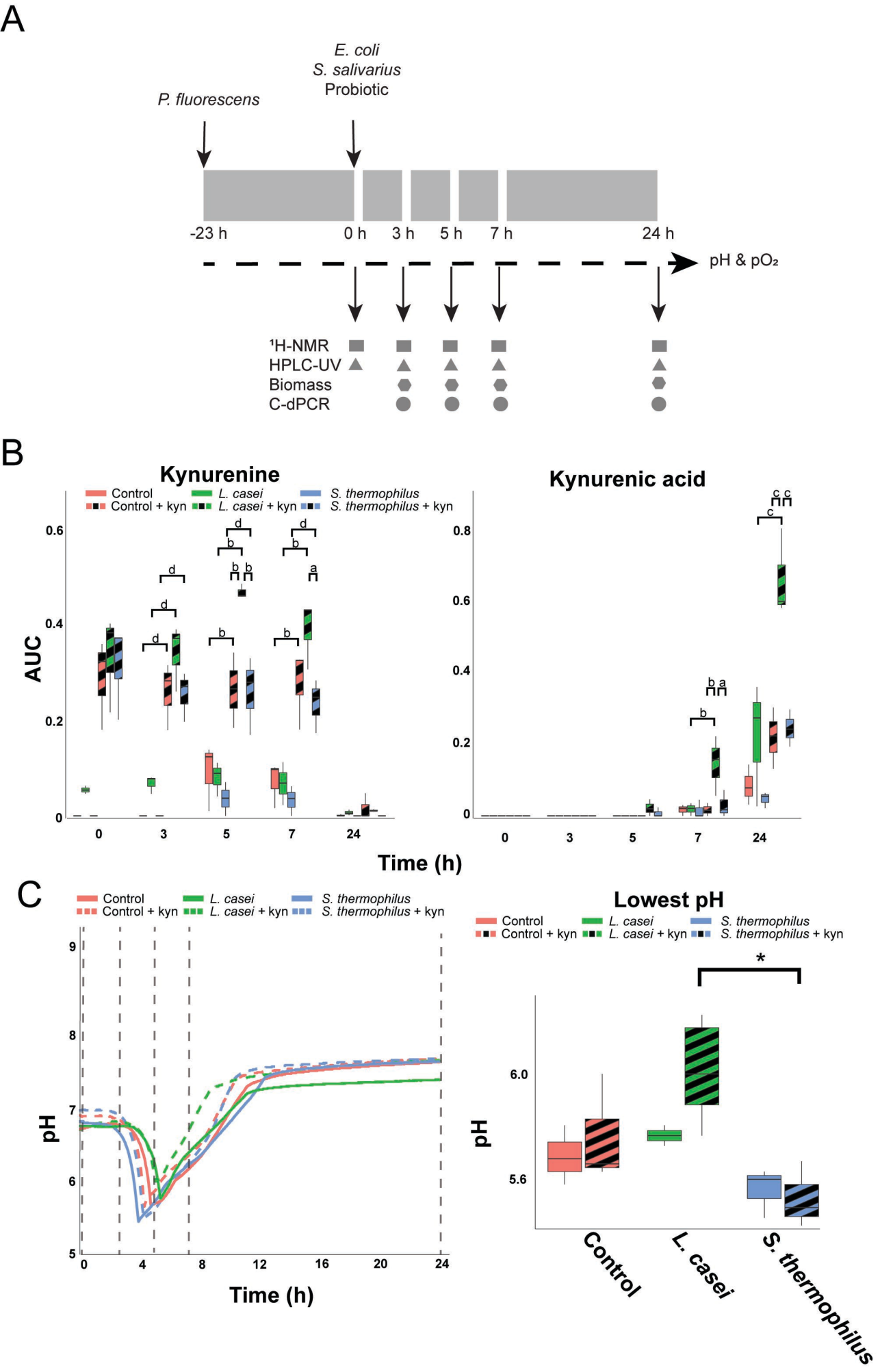
A
E. coli
S. salivarius
Probiotic
P. fluorescens
-23 h
0 h
3 h
5 h
7 h
24 h
pH & pO₂
¹H-NMR
HPLC-UV
Biomass
C-dPCR
B
Kynurenine
Control
Control + kyn
L. casei
L. casei + kyn
S. thermophilus
S. thermophilus + kyn
AUC
Kynurenic acid
Time (h)
C
pH
Time (h)
Lowest pH
Control
L. casei
S. thermophilus

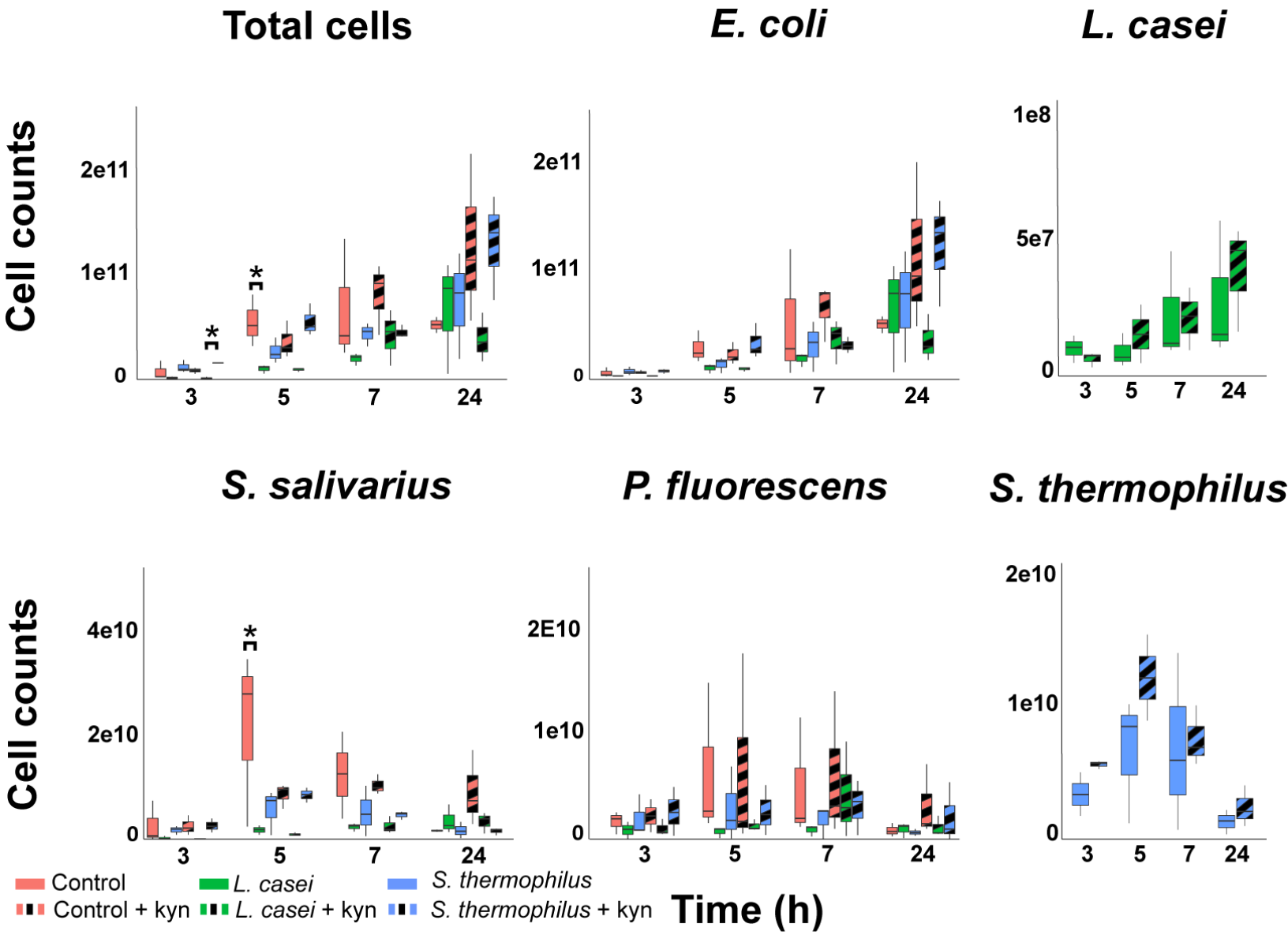
Total cells
E. coli
L. casei
S. salivarius
P. fluorescens
S. thermophilus
Cell counts
Cell counts
2e11
1e11
0
1e8
5e7
4e10
2e10
2E10
1e10
3
5
7
24
*
Control
Control + kyn
L. casei
L. casei + kyn
S. thermophilus
S. thermophilus + kyn
Time (h)

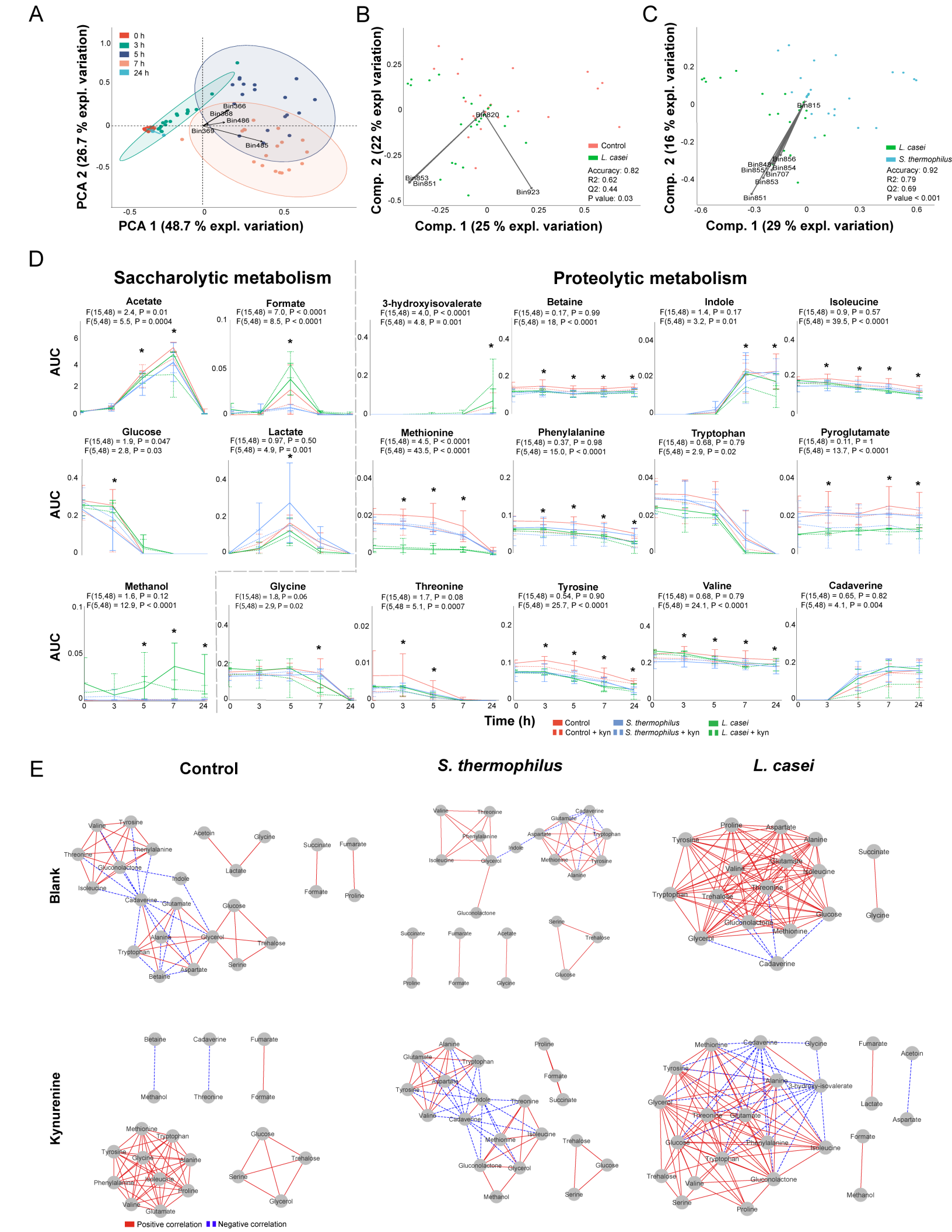
A
0 h
3 h
5 h
7 h
24 h
Bin366
Bin368
Bin486
Bin369
Bin485
PCA 2 (26.7 % expl. variation)
PCA 1 (48.7 % expl. variation)
B
Bin820
Bin853
Bin851
Bin923
Control
L. casei
Accuracy: 0.82
R2: 0.62
Q2: 0.44
P value: 0.03
Comp. 2 (22 % expl variation)
Comp. 1 (25 % expl. variation)
C
Bin815
Bin848
Bin855
Bin856
Bin854
Bin707
Bin853
Bin851
L. casei
S. thermophilus
Accuracy: 0.92
R2: 0.79
Q2: 0.69
P value < 0.001
Comp. 2 (16 % expl. variation)
Comp. 1 (29 % expl. variation)
D
Saccharolytic metabolism
Proteolytic metabolism
Acetate
F(15,48) = 2.4, P = 0.01
F(5,48) = 5.5, P = 0.0004
Formate
F(15,48) = 7.0, P < 0.0001
F(5,48) = 8.5, P < 0.0001
3-hydroxyisovalerate
F(15,48) = 4.0, P < 0.0001
F(5,48) = 4.8, P = 0.001
Betaine
F(15,48) = 0.17, P = 0.99
F(5,48) = 18, P < 0.0001
Indole
F(15,48) = 1.4, P = 0.17
F(5,48) = 3.2, P = 0.01
Isoleucine
F(15,48) = 0.9, P = 0.57
F(5,48) = 39.5, P < 0.0001
Glucose
F(15,48) = 1.9, P = 0.047
F(5,48) = 2.8, P = 0.03
Lactate
F(15,48) = 0.97, P = 0.50
F(5,48) = 4.9, P = 0.001
Methionine
F(15,48) = 4.5, P < 0.0001
F(5,48) = 43.5, P < 0.0001
Phenylalanine
F(15,48) = 0.37, P = 0.98
F(5,48) = 15.0, P < 0.0001
Tryptophan
F(15,48) = 0.68, P = 0.79
F(5,48) = 2.9, P = 0.02
Pyroglutamate
F(15,48) = 0.11, P = 1
F(5,48) = 13.7, P < 0.0001
Methanol
F(15,48) = 1.6, P = 0.12
F(5,48) = 12.9, P < 0.0001
Glycine
F(15,48) = 1.8, P = 0.06
F(5,48) = 2.9, P = 0.02
Threonine
F(15,48) = 1.7, P = 0.08
F(5,48 = 5.1, P = 0.0007
Tyrosine
F(15,48) = 0.54, P = 0.90
F(5,48) = 25.7, P < 0.0001
Valine
F(15,48) = 0.68, P = 0.79
F(5,48) = 24.1, P < 0.0001
Cadaverine
F(15,48) = 0.65, P = 0.82
F(5,48) = 4.1, P = 0.004
AUC
Time (h)
Control
Control + kyn
S. thermophilus
S. thermophilus + kyn
L. casei
L. casei + kyn
E
Control
S. thermophilus
L. casei
Blank
Kynurenine
Positive correlation
Negative correlation

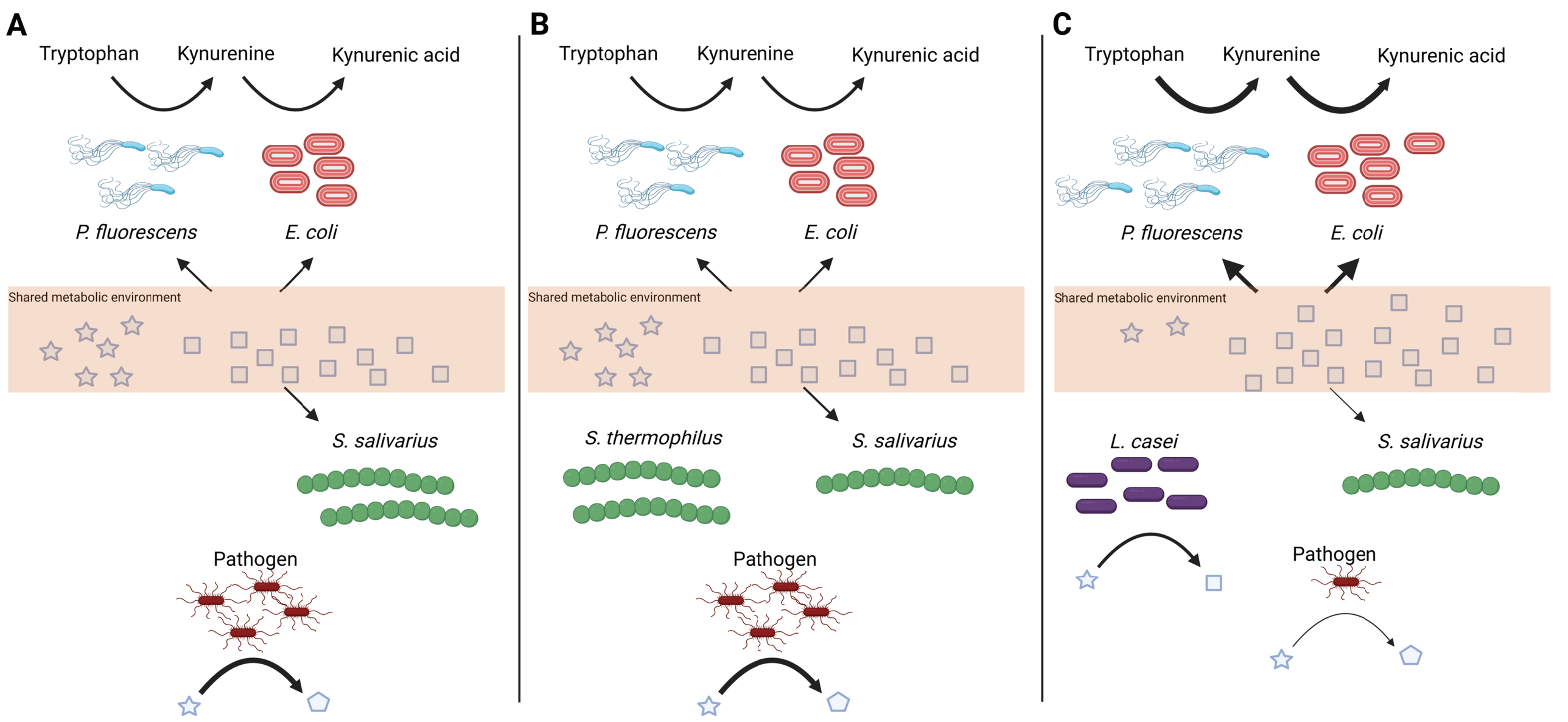
A
Tryptophan
Kynurenine
Kynurenic acid
P. fluorescens
E. coli
Shared metabolic environment
S. salivarius
Pathogen
B
Tryptophan
Kynurenine
Kynurenic acid
P. fluorescens
E. coli
Shared metabolic environment
S. thermophilus
S. salivarius
Pathogen
C
Tryptophan
Kynurenine
Kynurenic acid
P. fluorescens
E. coli
Shared metabolic environment
L. casei
S. salivarius
Pathogen